Fermi-liquid, non-Fermi-liquid, and Mott phases in iron pnictides and cuprates

Hiroshi Ishida[1] and Ansgar Liebsch[2]
[1]*College of Humanities and Sciences, Nihon University, Tokyo 156, Japan*
[2]*Institut für Festkörperforschung, Forschungszentrum Jülich, 52425 Jülich, Germany*
(Received 11 November 2009; revised manuscript received 18 January 2010; published 19 February 2010)

The role of Coulomb correlations in the iron pnictide LaFeAsO is studied by generalizing exact diagonalization dynamical mean-field theory to five orbitals. For rotationally invariant Hund's rule coupling a transition from a paramagnetic Fermi-liquid phase to a non-Fermi-liquid metallic phase exhibiting frozen moments is found at moderate Coulomb energies. For Ising-like exchange, this transition occurs at a considerably lower critical Coulomb energy. The correlation-induced scattering rate as a function of doping relative to half filling, i.e., $\delta=n/5-1$, where $n=6$ for the undoped material, is shown to be qualitatively similar to the one in the two-dimensional single-band Hubbard model which is commonly used to study strong correlations in high-T_c cuprates. In this scenario, the parent Mott insulator of LaFeAsO is the half-filled $n=5$ limit, while the undoped $n=6$ material corresponds to the critical doping region $\delta_c \approx 0.2$ in the cuprates, on the verge between the Fermi-liquid phase of the overdoped region and the non-Fermi-liquid pseudogap phase in the underdoped region.

DOI: 10.1103/PhysRevB.81.054513 PACS number(s): 71.20.Be

I. INTRODUCTION

The discovery of superconductivity in the iron-based pnictides[1–4] has recently led to an intense debate on the question whether Coulomb correlations in these materials play a role of similar importance as in the high-T_c cuprates.[5–40] Moreover, in contrast to the effective single-band character of the $3d_{x^2-y^2}$ states in the cuprates, the number of relevant d orbitals in the pnictides has also been a subject of discussion. In addition, because of the multiband character of the Fe $3d$ bands, the interplay of Coulomb repulsion, and Hund's rule coupling should be of crucial importance for the pnictides. Finally, while it is generally accepted that the non-Fermi-liquid pseudogap properties in the underdoped regime of the cuprates are associated with the vicinity to the Mott insulating phase, in the pnictides it is not yet clear whether there exists a nearby Mott phase in the range of realistic Coulomb and exchange energies.

To study the effect of Coulomb correlations in iron pnictides, various groups[5,16–18,20,21,25,32,33,37] have applied single-site dynamical mean-field theory[41] (DMFT). Depending on the details of the single-particle Hamiltonian and the magnitude of Coulomb and exchange energies, weakly or strongly correlated solutions were found. In the present work we extend exact diagonalization[42,43] (ED) DMFT to five orbitals in order to investigate correlation effects in LaFeAsO as a function of Coulomb energy. The single-particle properties are described in terms of a five-band tight-binding Hamiltonian.[24] Each d orbital hybridizes with two bath levels, giving 15 levels in total. The five baths are coupled indirectly via the interorbital $3d$ Coulomb and exchange interactions. Thus, the Hilbert space is extremely large and finite-size effects are effectively reduced. The advantage of this multiorbital ED/DMFT approach is that it is particularly useful at low temperatures and that it can handle large Coulomb energies and full Hund exchange. As will be discussed below, the latter feature is of special importance in the pnictides since Hund's rule coupling leads to electronic properties that differ qualitatively from those obtained for the more approximate Ising-like exchange treatment. The sensitive role of exchange interactions in the pnictides was also noted in several previous papers.[5,16,25,32]

The main result of this work is the identification of a paramagnetic Fermi-liquid to non-Fermi-liquid transition at moderate Coulomb energies, $U_c \approx 3$ eV ($J=0.75$ eV), i.e., well below the overall width of the Fe $3d$ bands, $W \approx 4.5$ eV. This incoherent metallic phase extends up to rather large values of U (>6 eV if J is kept fixed at 0.75 eV). It is associated with the formation of local moments and with substantial low-frequency scattering rates in all $3d$ bands. Below this transition, all bands exhibit strong correlation-induced effective mass enhancement. These properties are intimately related to the multiband nature of LaFeAsO and the Hund's rule coupling among the Fe $3d$ subbands. A similar spin-freezing transition had been found recently by Werner *et al.*[44] in a fully degenerate three-band model. Within the present five-band system, a Mott phase is not obtained below $U=6$ eV. Thus, correlation effects in LaFeAsO appear to be related to the formation of local moments within the non-Fermi-liquid phase, and not to the vicinity of a Mott insulating phase.

On the other hand, LaFeAsO readily turns into a Mott insulator at realistic Coulomb energies in the hypothetical limit of one-hole doping, i.e., $n=5$. The $3d$ bands then become half-filled and split into lower and upper Hubbard bands. At intermediate hole doping, non-Fermi-liquid behavior dominates, while for electron doping ($n>6$) the system becomes a normal Fermi-liquid. These results suggest a remarkable correspondence between the multiband compound LaFeAsO and the two-dimensional single-band Hubbard model. Indeed, if the correlation-induced scattering rate is plotted as a function of doping relative to half-filling, i.e., $\delta=n/5-1$ ($n=6$ for pure LaFeAsO), both systems exhibit the same sequence of phases for increasing δ: a Mott insulator at half-filling, a non-Fermi-liquid phase up to a critical doping of the order of $\delta_c \approx 0.15 \ldots 0.20$, and a weakly correlated Fermi-liquid for $\delta > \delta_c$. In this scenario, the paramagnetic

phase diagrams of iron pnictides and cuprates are strikingly similar, with LaFeAsO ($\delta=0.2$) located slightly on the overdoped side above critical doping. As a result, the system exhibits a clear asymmetry with respect to doping. Whereas electron doping beyond $n=6$ ($\delta>0.2$) reinforces Fermi-liquid properties, hole doping $n<6$ ($\delta<0.2$) enhances bad-metallic behavior. Although the real material is undoubtedly more complex because of doping-dependent single-particle properties and the presence of antiferromagnetism[4] at $n=6$, we believe that the above picture nevertheless provides a useful perspective for the role of correlation effects in iron pnictides in comparison with analogous physics in the cuprates.

If exchange interactions among Fe $3d$ electrons are approximated in terms of Ising-like exchange, i.e., by neglecting spin-flip and pair-exchange processes, the Fermi-liquid to non-Fermi-liquid transition still exists, but the critical value of U is shifted down to about 2 eV (assuming $J=U/4$) and the transition is more abrupt. Similar qualitative changes from Hund to Ising exchange were found previously also for the Mott transition in two-band Hubbard models.[45,46]

Because of the strong hybridization between Fe $3d$ and As $4p$ and O $2p$ states, there are indications that an accurate Wannier representation should encompass not only d but also p type basis functions, even if Coulomb correlations are explicitly only included among the $3d$ orbitals.[18,19,21,25,30,32] A particular consequence of dp hybridization is that the effective $3d$ Coulomb interaction is considerably reduced. Moreover, Coulomb interactions among different d states are differently screened, giving rise to nonisotropic intraorbital and interorbital matrix elements.[19,32] The present approach is general in the sense that these choices only affect the single-particle Hamiltonian and not the evaluation of the d electron self-energy matrix. Nevertheless, in this initial five-orbital ED/DMFT study we use, for simplicity, a purely d electron tight-binding picture[24] in order to elucidate the nature of the transition from Fermi-liquid to non-Fermi-liquid behavior. A more detailed investigation within a dp formulation is planned for future work. As in previous papers,[5,16–18,20,21,25,32,33,37] we focus here on the paramagnetic phase.

The outline of this paper is as follows. In Sec. II we discuss several theoretical details concerning the single-particle properties of LaFeAsO and the ED/DMFT procedure that is used to evaluate the Fe $3d$ self-energy components. In Sec. III we analyze the results, with particular focus on the differences obtained for Hund and Ising exchange. Sec. III A discusses the neutral system, whereas the effect of doping and the analogy between pnictides and cuprates are the subject of Sec. III B. Sec. IV contains the summary.

II. MULTIBAND ED/DMFT

In this section we briefly outline the theoretical details of the multiband ED/DMFT approach used in this work. The focus is on the role of Coulomb correlations within the Fe $3d$ subbands of LaFeAsO. The single-particle properties are described in terms of the five-band tight-binding Hamiltonian $H(\mathbf{k})$ which was recently derived by Graser *et al.*[24] for a single plane of Fe atoms from an accurate fit to the density-functional results by Cao *et al.*[47] The low-energy part of these bands are in excellent agreement with analogous calculations by Singh *et al.*[48] The basis functions are d_{xz}, d_{yz}, $d_{x^2-y^2}$, d_{xy}, and $d_{3z^2-r^2}$, where the x and y axes point along Fe nearest-neighbor directions. The first three of these orbitals comprise the t_{2g} subset, the remaining two orbitals represent the e_g subset. Hopping up to fifth nearest neighbors was included in the tight-binding fit. The onsite energies are $E_{xz,yz}=0.13$ eV, $E_{x^2-y^2}=-0.22$ eV, $E_{xy}=0.3$ eV, and $E_{z^2}=-0.211$ eV. Thus the $d_{xz,yz,xy}$ levels lie 0.2…0.4 eV above the $d_{x^2-y^2,z^2}$ levels. The hopping parameters are given in the Appendix of Ref. 24 and the one-electron band structure corresponding to this Hamiltonian is shown in Fig. 5 of this reference.

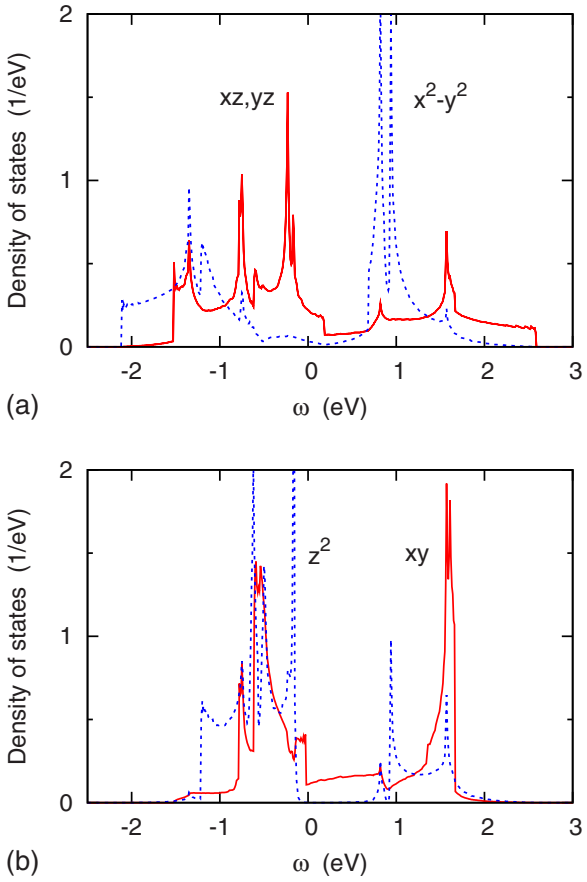

FIG. 1. (Color online) Density of states components of LaFeAsO for tight-binding band structure derived in Ref. 24. (a) t_{2g} components $\rho_{xz,yz}$ and $\rho_{x^2-y^2}$, (b) e_g components ρ_{xy} and ρ_{z^2}.

The Fe $3d$ density of states components are shown in Fig. 1. For symmetry reasons, the d_{xz} and d_{yz} components are degenerate. The widths of the t_{2g} and e_g bands are approximately 3.0 and 4.0 eV, respectively. The total band width is about 4.5 eV. All Fe $3d$ bands exhibit a pronounced bonding-antibonding splitting, with a deep pseudogap at small positive energies, due to the hybridization with the neighboring LaAsO layers. In the absence of correlations, the occupancies of these bands are: $n_{xz,yz}=0.58$, $n_{x^2-y^2}=0.53$, $n_{xy}=0.52$, and $n_{z^2}=0.78$. Note that these occupancies do not reflect the crystal-field splitting among the onsite energies because of

the complex shape of the density of states components. In particular, the bands of d_{z^2} character are considerably more occupied than those of $d_{x^2-y^2}$ character, despite the fact that $E_{z^2} > E_{x^2-y^2}$. A similar situation exists in the layer compound Na_xCoO_2, where $n_{e'_g} > n_{a_g}$ although $E_{e'_g} > E_{a_g}$.[49]

Previously, we have used finite-temperature ED/DMFT to investigate correlation effects in t_{2g} three-band transition metal oxides such as Ca_2RuO_4,[50] Na_xCoO_2,[49,51] $LaTiO_3$,[52] and V_2O_3.[53] It was shown that, in these systems, accurate projections of the lattice Green's function onto a finite cluster consisting of three impurity levels and six bath levels (two bath levels per t_{2g} orbital) can be achieved, yielding an overall cluster size $n_s=9$. Since the different baths are indirectly coupled via the $3d$ interorbital Coulomb and exchange interactions, the spacing between excitation energies is rather small, so that finite-size effects are greatly diminished. Here, we generalize this approach to five impurity orbitals, each coupled to two bath levels, i.e., $n_s=15$.

Denoting the tight-binding matrix elements by $H_{mn}(\mathbf{k})$ the interacting Hamiltonian is given by:

$$H = \sum_{mn\mathbf{k}\sigma} H_{mn}(\mathbf{k}) c^+_{m\mathbf{k}\sigma} c_{n\mathbf{k}\sigma} + \sum_{im} U n_{im\uparrow} n_{im\downarrow} + \sum_{im<m'\sigma\sigma'} (U' - J\delta_{\sigma\sigma'}) n_{im\sigma} n_{im'\sigma'} - \sum_{im\neq m'} J' [c^+_{im\uparrow} c_{im\downarrow} c^+_{im'\downarrow} c_{im'\uparrow} + c^+_{im\uparrow} c^+_{im\downarrow} c_{im'\uparrow} c_{im'\downarrow}], \quad (1)$$

where $c^{(+)}_{im\sigma}$ are annihilation (creation) operators for electrons on site i in orbital m with spin σ and $n_{im\sigma}=c^+_{im\sigma}c_{im\sigma}$. $c^{(+)}_{\mathbf{k}m\sigma}$ are the corresponding Fourier components. The intraorbital and interorbital Coulomb energies are denoted by U and U'. The exchange integral is J, where $U'=U-2J$ because of rotational invariance. Spin-flip and pair-exchange terms are denoted explicitly by J'. In the case of isotropic Hund exchange, one has $J'=J$. In the case of Ising-like exchange these terms are neglected, i.e., $J'=0$.

The aim of the five-orbital single-site DMFT calculation is to derive the local self-energy matrix $\Sigma_{mn}(\omega)$ which describes the modification of the single-particle bands due to Coulomb interactions. The local lattice Green's function is given by

$$G_{mn}(i\omega_n) = \sum_{\mathbf{k}} [i\omega_n + \mu - H(\mathbf{k}) - \Sigma(i\omega_n)]^{-1}_{mn}, \quad (2)$$

where $\omega_n=(2n+1)\pi T$ are Matsubara frequencies and μ is the chemical potential. Since we consider paramagnetic systems, the spin index of G and Σ is omitted. As a result of the symmetry properties of $H_{mn}(\mathbf{k})$, the density of states matrix is diagonal: $\rho_{mn}(\omega)=\delta_{mn}\rho_m(\omega)$. Local Coulomb interactions preserve this symmetry, so that G_{mn} and Σ_{mn} are also diagonal. We denote these components by $G_m(i\omega_n)$ and $\Sigma_m(i\omega_n)$. We point out that, because of the nondiagonal nature of $H(\mathbf{k})$, each G_m component is influenced by all components Σ_m.

For the purpose of the quantum impurity calculation within DMFT it is necessary to first remove the self-energy from the central site. This step yields the impurity Green's function

$$G_{0,m}(i\omega_n) = [G_m(i\omega_n)^{-1} + \Sigma_m(i\omega_n)]^{-1}. \quad (3)$$

Within ED/DMFT the lattice impurity Green's function G_0 is approximated in terms of an Anderson impurity model for a cluster consisting of impurity levels $\varepsilon_{m=1\ldots5}$ and bath levels $\varepsilon_{k=6\ldots15}$, which are coupled via hopping matrix elements V_{mk}. Thus, $G_{0,m}(i\omega_n) \approx G^{cl}_{0,m}(i\omega_n)$, where

$$G^{cl}_{0,m}(i\omega_n) = \left(i\omega_n + \mu - \varepsilon_m - \sum_{k=6}^{15} \frac{|V_{mk}|^2}{i\omega_n - \varepsilon_k} \right)^{-1}. \quad (4)$$

Since $G^{cl}_{0,m}$ is diagonal in orbital indices, each impurity level couples to its own bath containing two levels: orbital 1 couples to bath levels 6 and 7, orbital 2 to bath levels 8 and 9, etc. Each of the four independent functions $G^{cl}_{0,m}(i\omega_n)$ therefore involves five adjustable parameters: one impurity level, two bath levels, and two hopping elements. These parameters are found by using a standard minimization procedure. The quality of these fits using five parameters is very good, as shown in several previous works.[53,54]

As a result of the ED quantum impurity calculation one obtains the finite-temperature cluster Green's function which is also diagonal: $G^{cl}_m(i\omega_n)$. In analogy to Eq. (3) the cluster self-energy is given by

$$\Sigma^{cl}_m(i\omega_n) = G^{cl}_{0,m}(i\omega_n)^{-1} - G^{cl}_m(i\omega_n)^{-1}. \quad (5)$$

The important physical assumption within DMFT is now that this cluster self-energy provides an adequate representation of the self-energy of the extended solid, i.e., $\Sigma^{cl}_m(i\omega_n) \approx \Sigma_m(i\omega_n)$, which is then used in Eq. (2) to derive the lattice Green's function in the next iteration step. Further details can be found in Ref. 51.

Since the cluster Hamiltonian is extremely sparse (typically only 20 to 30 off-diagonal elements per row), the quantum impurity calculation is conveniently carried out by using the Arnoldi algorithm.[55] The largest spin sector corresponds to $(n_\uparrow,n_\downarrow)=(7,8)$, giving matrix dimension $[15!/(7!8!)]^2 = 6435^2$. To reduce storage requirements, we have rewritten our multiorbital ED/DMFT code so that large basis vectors of size 2^{2n_s} are avoided by keeping only vectors of size 2^{n_s}. Moreover, the Arnoldi scheme is readily parallelized. Thus, using 32 processors the largest Hamiltonian subblock requires less than 1 GB storage. Since the spacing between excited states is very small, at finite temperatures a large number of states may contribute to the cluster Green's function. To reduce computational time in this first five-band ED study, we perform the DMFT calculation at $T=0.01$ eV, but retain only the lowest few states, making sure that ground-state degeneracies are properly treated. Using 32 processors, one iteration then takes of the order of one to four hours.

III. RESULTS AND DISCUSSION

A. Undoped LaFeAsO

An important consequence of local Coulomb interactions is the rearrangement of electrons among subbands. Figure 2

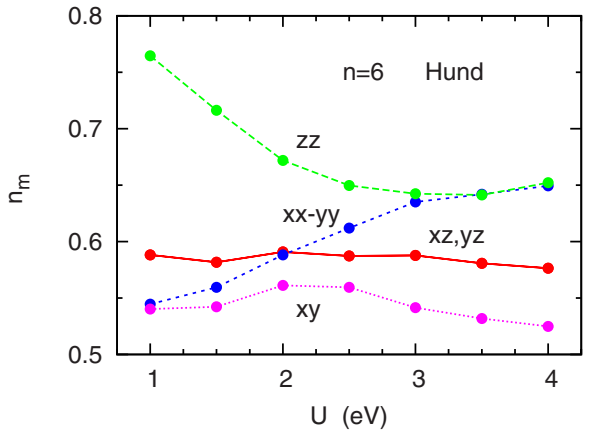

FIG. 2. (Color online) Fe $3d$ orbital occupancies (per spin) as functions of Coulomb interaction for $n=6$, with $J=U/4$ for $U \leq 3$ eV and $J=0.75$ eV for $U>3$ eV; Hund exchange.

shows the variation of the Fe $3d$ orbital occupancies with U at $n=6$ total occupancy. The precise values of U and J for LaFeAsO depend sensitively on the basis functions used for the $3d$ Hamiltonian.[18,20,21,32] In the range $U \leq 3$ eV we chose $J=U/4$. For illustrative purposes we also show results for larger U. In this range J is kept constant at 0.75 eV, in order to avoid unrealistically large Hund parameters. A charge flow from d_{z^2} to $d_{x^2-y^2}$ is seen to take place, thereby reducing the orbital polarization of the uncorrelated bands. The occupancies of the $d_{xz,yz,xy}$ orbitals are less strongly affected by correlations. The results shown are for full Hund coupling. Ising exchange yields a similar charge rearrangement predominantly between d_{z^2} and $d_{x^2-y^2}$ orbitals with only slightly larger modifications of the $d_{xz,yz,xy}$ occupancies than seen in Fig. 2. Near $U=2.5$ eV, all $3d$ occupancies are within about 10% of the average occupancy 0.6. The origin of the unusual reduced d_{z^2,x^2-y^2} orbital polarization is the complex bonding-antibonding shape of the density of states which yields $n_{z^2} > n_{x^2-y^2}$ although $E_{z^2} > E_{x^2-y^2}$. A correlation-induced reduction in orbital polarization is also found in Na_xCoO_2 which exhibits a similar pseudogap in the density of states as a result of the strong $3d-2p$ hybridization in the planar geometry.[49]

To illustrate the effect of Coulomb correlations on the Fe $3d$ bands in more detail, we show in Fig. 3 the self-energy components as functions of Matsubara frequency. In the case of Hund coupling, the initial slope of $\mathrm{Im}\,\Sigma_m(i\omega_n) \sim \omega_n$ increases up to about $U=3$ eV, until the quasiparticle weights are reduced to about $0.15 \ldots 0.3$. Beyond this Coulomb energy, the self-energy components exhibit a finite onset of $-0.3 \ldots -0.6$ eV, indicating that states at the Fermi level acquire a finite lifetime. Since this onset is much larger than what is expected due to finite temperature, it implies a breakdown of Fermi-liquid behavior. The loss of coherence is strongest for d_{xy} and weakest for d_{z^2}. Ising exchange also gives rise non-Fermi-liquid behavior, except that the onset occurs at about $U=2$ eV, i.e., at considerably lower Coulomb energy than for Hund exchange.

Figure 4 shows the orbital dependent quasiparticle weights $Z_m = 1/[1 - \mathrm{Im}\, d\Sigma_m(i\omega)/d\omega|_{\omega \to 0}]$ as functions of Coulomb energy for Hund exchange. Despite the different $3d$

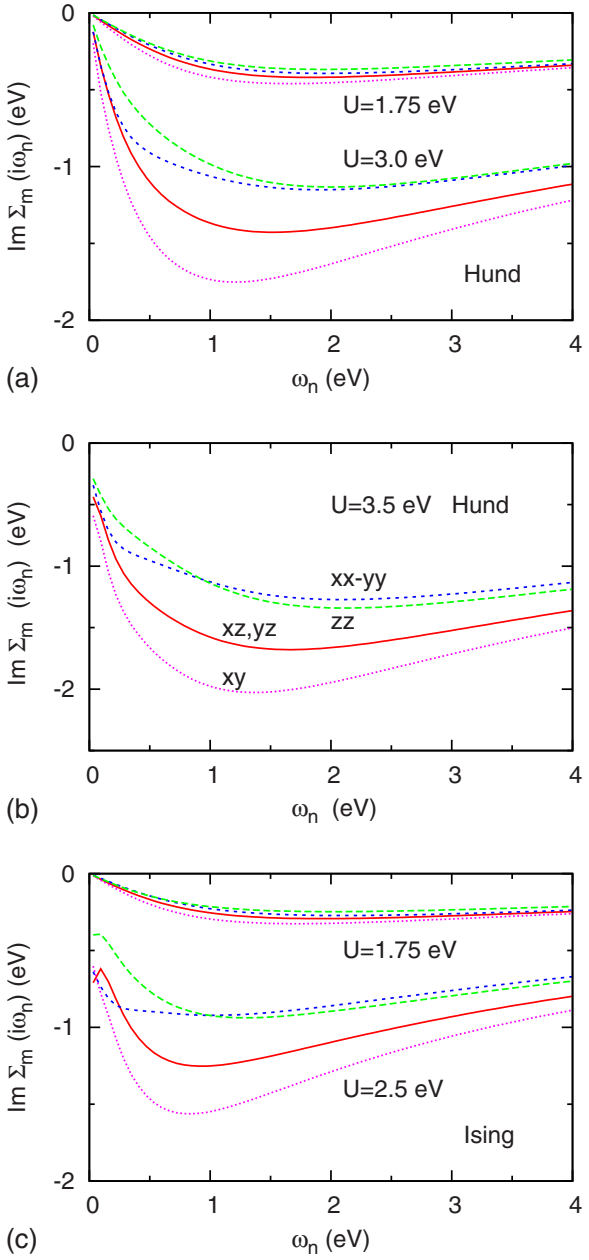

FIG. 3. (Color online) Imaginary part of self-energy components $\Sigma_m(i\omega_n)$ as function of Matsubara frequency for several Coulomb energies. (a) and (b): Hund coupling; (c) Ising exchange. The color coding is defined in panel (b).

orbital occupancies and different t_{2g} and e_g band widths, all five bands are seen to exhibit a similar reduction in Z_m with increasing U. Ising exchange yields a slightly steeper decrease in Z_m up to about $U=2$ eV, beyond which all self-energy components show a finite onset.

There exists strong experimental evidence that Fe pnictides exhibit an orbital dependent effective mass enhancement and an concomitant narrowing of quasiparticle bands of about a factor of 2 to 3.[31,34,56,57] According to the results shown in Fig. 4, these experimental findings are compatible with the present five-orbital picture if $U \approx 2.0 \ldots 2.5$ eV with $J \approx U/4$ and full Hund's rule coupling. The system would then be just below the Fermi-liquid to non-Fermi-liquid

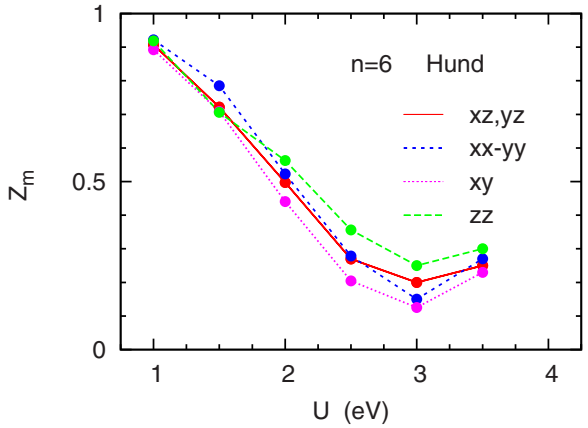

FIG. 4. (Color online) Quasiparticle weights Z_m of Fe $3d$ orbitals as functions of Coulomb interaction for $n=6$; Hund exchange.

phase boundary. For Ising exchange, on the other hand, these Coulomb and exchange parameters would imply non-Fermi-liquid behavior. The above small values of U evidently reflect the fact that, in a purely $3d$ electron description, screening via As and O p states greatly reduces the Fe $3d$ Coulomb interaction. Correspondingly larger U are appropriate within a more refined dp description.[18,21,30,32,33]

Figure 5 shows the variation of the low-frequency scattering rates $\gamma_m = -\mathrm{Im}\,\Sigma_m(i\omega \to 0)$ with Coulomb energy. For Hund as well as Ising exchange, the onset of non-Fermi-liquid occurs for all bands at the same critical U. Whereas Ising coupling leads to a sudden rise near $U \approx 2$ eV, Hund exchange shows a smoother increase near $U \approx 3$ eV. These results are consistent with previous ones for a degenerate two-band model[45] which showed that Ising coupling yields a lower critical Coulomb energy and a change from a continuous to a first-order transition. The damping rates for Ising coupling near $U=2.5$ eV are about $0.4 \ldots 0.7$ eV, in qualitative agreement with quantum Monte Carlo (QMC) results in Refs. 5 and 32. For Hund coupling near $U=3.5$ eV they are of similar magnitude. They continue to rise at larger U and indicate increasing orbital differentiation, with larger damping for $d_{xy,xz,yz}$ than for $d_{x^2-y^2,z^2}$.

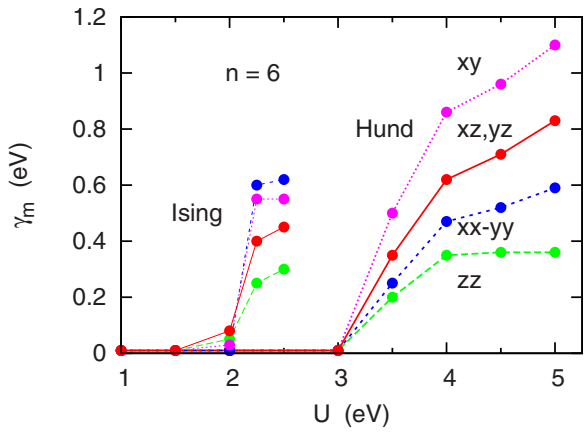

FIG. 5. (Color online) Orbital-dependent low-frequency scattering rates γ_m as functions of Coulomb interaction for Hund and Ising exchange.

The transition from coherent to incoherent metallic behavior should also manifest itself in the temperature variation of the Fe $3d$ self-energy. This has been studied recently for $LaFeAsO_{1-x}F_x$ at $x=0.1$ within continuous-time QMC DMFT for full Hund exchange.[25] The coherence temperature was shown to be a highly sensitive function of J, becoming extremely small for $J \approx 0.7$ eV, which is close to the value assumed here ($J=0.75$ eV for $U>3$ eV).

To explore the origin of the Fermi-liquid to non-Fermi-liquid transition we have evaluated the spin-spin correlation function $C_{mz}(\tau) = \langle S_{mz}(\tau) S_{mz}(0) \rangle$, where τ denotes the imaginary time. Figure 6 shows these orbital dependent functions for several Coulomb energies and Hund coupling. At low values of U, the $C_{mz}(\tau)$ decay to zero, as expected for a Fermi-liquid. The orbital components of the spin susceptibility

$$\chi_m \sim \int_0^\beta d\tau \langle S_{mz}(\tau) S_{mz}(0) \rangle, \tag{6}$$

are then independent of temperature, indicating Pauli behavior. With increasing U, the decay becomes less rapid and finite values are approached at large τ (for $\tau \ll \beta = 1/T$), demonstrating the formation of local moments S_m simultaneously in all subbands. The susceptibility components are then proportional to β, so that $\chi_m \sim S_m(S_m+1)/T$, as expected for Curie-Weiss behavior. As shown in Fig. 7, for Ising coupling the formation of frozen moments sets in at much lower Coulomb energies.

A similar spin-freezing transition was recently found by Werner *et al.*[44] for a fully degenerate three-band model near $n=2$ occupancy. Using continuous-time QMC as impurity solver, the paramagnetic $U-n$ phase diagram was shown to exhibit Fermi-liquid properties at small U. For increasing U and $n>1.5$, an incoherent metallic phase with local moments appears, which is then replaced by a Mott insulating phases at integer occupancies $n=2$ and 3. Beyond the critical value of U, the low-frequency limit of the self-energy exhibits a finite onset of similar magnitude as shown here in Fig. 5. In the present five-band study, we find in addition that this transition changes approximately from continuous to first-order when Hund exchange is replaced by Ising-like coupling.

To illustrate the correlation-induced transfer of spectral weight in LaFeAsO we show in Figs. 8(a) and 8(b) the $3d$ spectral distributions for two Coulomb energies and Hund coupling. For simplicity we plot here the ED cluster spectra since they do not require analytic continuation to real frequencies. The main effect at $U=1.75$ eV is the band narrowing both below and above E_F. In addition, spectral weight is shifted below the bottom of the $3d$ bands, indicating the formation of weak lower Hubbard bands. At $U=3$ eV, spectral weight in the occupied part of the $3d$ bands is greatly reduced and the Hubbard bands are much more prominent. Since there is little experimental evidence for any significant lower Hubbard bands, the above results imply that U within the present five-band description should be approximately $2.0 \ldots 2.5$ eV, where the precise value depends on the magnitude of J. The unoccupied states are also shifted closer to E_F, but there is no evidence of any upper Hubbard peaks.

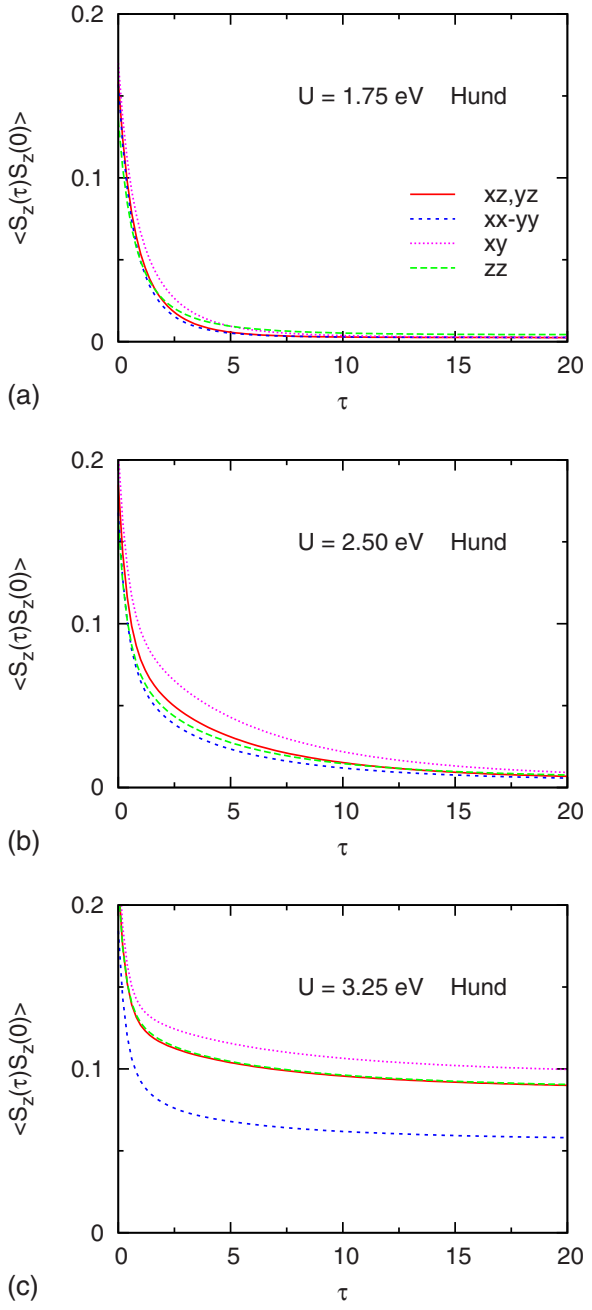

FIG. 6. (Color online) Variation of orbital dependent spin-spin correlation functions with imaginary time τ for three Coulomb energies and Hund coupling. (a) $U=1.75$ eV, (b) $U=2.5$ eV, and (c) $U=3.25$ eV.

Note that the lower Hubbard bands are very broad. This is related to large uncorrelated band width and to the multiplet structure induced by Hund's rule coupling. The spectra for Ising exchange shown in panel (c) are qualitatively similar. Many small differences arise because of the absence of spin flip and pair hopping exchange processes. The different multiplet structures associated with Hund and Ising coupling will be considered in more detail elsewhere.

The above results demonstrate the importance of a proper treatment of exchange interactions. For instance, if because of *pd* screening realistic values of U and J for LaFeAsO are

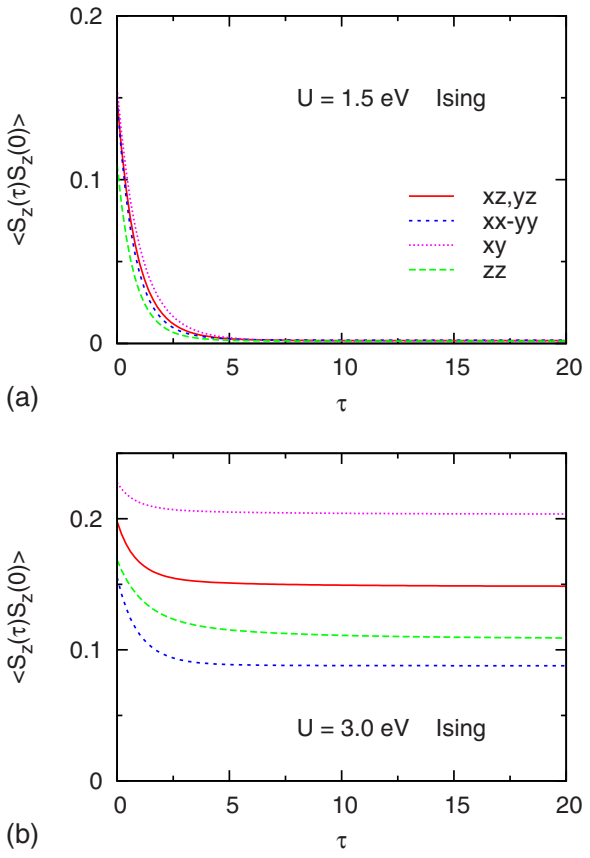

FIG. 7. (Color online) Variation of orbital dependent spin-spin correlation functions with imaginary time τ for two Coulomb energies and Ising exchange. (a) $U=1.5$ eV and (b) $U=3.0$ eV; $J=U/4$.

approximately 2.0…2.5 eV and $J\approx U/4$, respectively, full Hund coupling suggests that the system is moderately strongly correlated, with $3d$ effective mass enhancements of the order of $m^*/m=1/Z_m\approx 2\ldots 3$. In contrast, if spin-flip and pair-exchange processes are ignored (as is usually done in Hirsch-Fye QMC calculations to avoid sign problems, e.g., in Refs. 20, 21, and 33), the same Coulomb and exchange parameters suggest that system has crossed the boundary toward non-Fermi-liquid behavior, with strongly reduced lifetimes of electronic states close to E_F. It would be interesting to inquire whether a *dp* formulation of $H(\mathbf{k})$ yields a similar qualitative difference between Hund and Ising exchange.

At sufficiently large Coulomb energies, $n=6$ integer occupancy should eventually lead to a Mott insulating phase. We have increased U up to 6 eV while keeping $J=0.75$ eV constant. Both for Hund and Ising coupling, the system evolves toward an orbital selective phase, where the $d_{xz,yz,xy}$ subset is either in or close to an insulating phase and the $d_{x^2-y^2,z^2}$ subset remains in the strongly incoherent metallic state.[58] Thus, for realistic Coulomb and exchange we conclude that in the present five-orbital ED/DMFT description the system is far below the $n=6$ Mott insulating region. Orbital selective phases in five-band systems at $n=6$ occupancy, with subbands split via a crystal field, were also found in Refs. 27 and 59.

We close this subsection by pointing out that several papers have recently discussed the role of coexisting itinerant

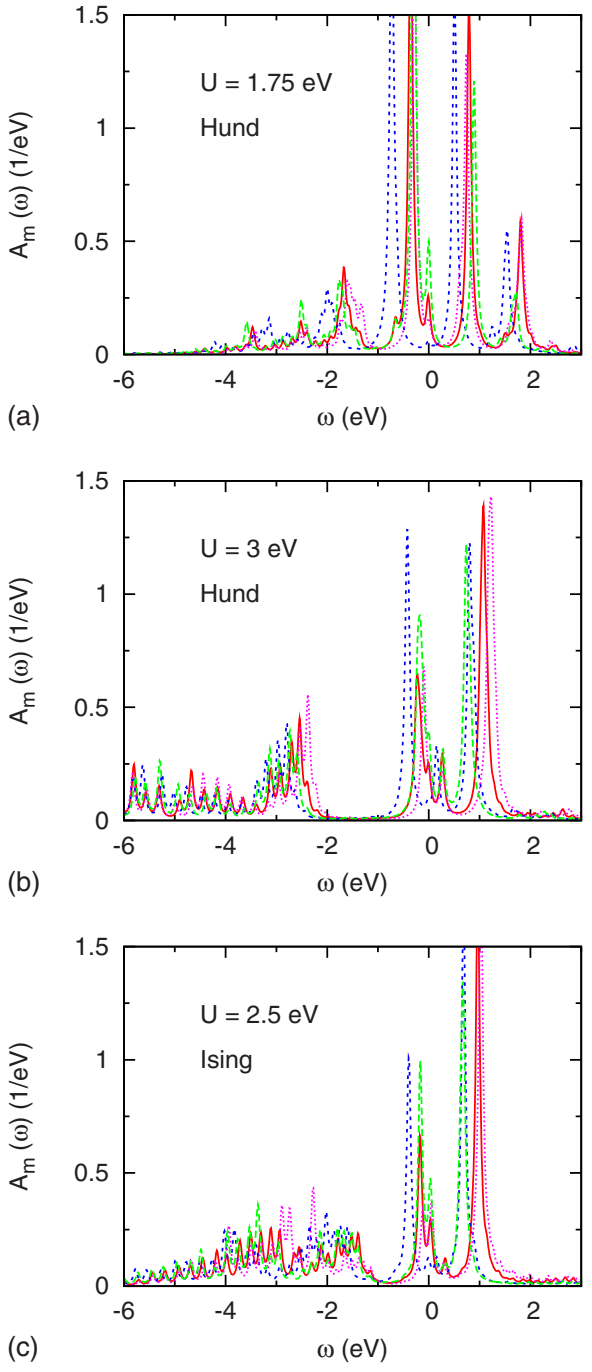

FIG. 8. (Color online) Spectral distributions of Fe $3d$ subbands for (a) $U=1.75$ eV and (b) $U=3$ eV; Hund coupling; (c) $U=2.5$ eV: Ising exchange; with $J=U/4$ and 0.05 eV broadening.

and localized electrons in iron pnictides.[7,10,26–28,36] A simple system which exhibits this kind of coexistence is the half-filled two-band model where the narrow band is Mott localized while the wide band is still metallic.[46,60–62] Coulomb interactions between these two types of electrons give rise to bad-metallic behavior in the itinerant band, with a finite scattering rate and a pseudogap at E_F in the case of Ising exchange[60] and marginal Fermi-liquid behavior in the case of full Hund coupling.[61,62] As we have seen above, the important feature of FeAsLaO at $n=6$ occupancy is that the spin-freezing transition occurs simultaneously in all five d bands, far below the Mott transition. Thus, in the range of Coulomb and exchange energies of interest, all subbands have similar occupancies, effective masses, and low-frequency scattering rates. The subbands therefore do not split into itinerant and localized subsets. Only at much larger U, the $d_{xz,yz,xy}$ and $d_{x^2-y^2,z^2}$ bands gradually tend toward 0.5 and 0.75 occupancy.

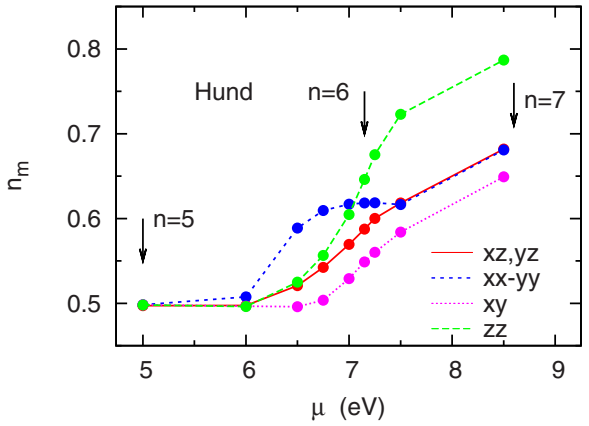

FIG. 9. (Color online) Fe $3d$ orbital occupancies as functions of chemical potential for $U=2.5$ eV with $J=0.625$ eV and Hund coupling. The arrows indicate the values of μ associated with integer total occupancies.

B. Doped LaFeAsO: correspondence between pnictides and cuprates

The results discussed above are for paramagnetic, undoped LaFeAsO, with Fe $3d$ occupancy $n=6$. To illustrate the effect of electron and hole doping we show in Fig. 9 the orbital occupancies as functions of chemical potential at fixed $U=2.5$ eV. In order to elucidate the doping variation of many-body properties, the one-electron Hamiltonian is kept unchanged. The doping range extends from one hole to one electron. (At half-filling $n=5$, the chemical potential is $\mu=4.5U-10J=5$ eV.) Evidently, the degree of orbital polarization depends strongly on the total occupancy. For $n=5$, all d bands become half-filled and some orbital components $\mathrm{Im}\,\Sigma_m(i\omega_n)$ are proportional to $1/\omega_n$. The spectral distributions reveal that the system then is a Mott insulator where all d bands are split into lower and upper Hubbard peaks.

In the case of electron doping, all orbital occupancies increase in a similar fashion. At $n=7$, the self-energies (not shown) indicate that the system is a weakly correlated Fermi-liquid. Even for Ising exchange, the quasiparticle weights are in the range $Z_m=0.26\ldots0.56$. These properties differ strikingly from those discussed above at $n=6$, where under the same interaction conditions the system is much closer to bad-metallic behavior. Thus, the Fermi-liquid to non-Fermi-liquid phase boundary for $n=7$ is shifted to larger values of U. These results suggest a fundamental asymmetry of LaFeAsO with respect to doping. For hole doping, bad-metallic behavior should increase, while electron doping reinforces Fermi-liquid properties. This behavior is consistent with results for the three-band model[44] where the Fermi-liquid to non-Fermi-liquid phase boundary was also found to shift to larger U as

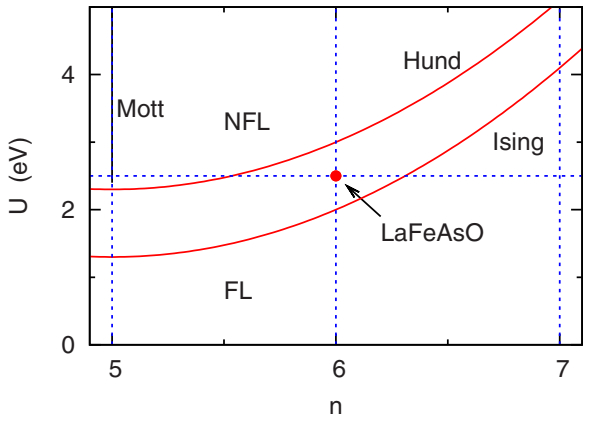

FIG. 10. (Color online) Schematic phase diagram for doped LaFeAsO. Red solid curves: boundaries between Fermi-liquid and non-Fermi-liquid phases for Hund and Ising exchange. At half-filling ($n=5$) a Mott insulating phase exists down to rather small U. The undoped material at $n=6$ with moderate $U\approx 2.5$ eV is a Fermi-liquid for Hund coupling, but an incoherent metal for Ising exchange. The $n=6$ Mott phase is located at $U>6$ eV.

the occupancy moves farther away from half-filling.

On the basis of the above results we obtain the paramagnetic $U-n$ phase diagram shown in Fig. 10, where, for $U=2.5$ eV and $J=U/4$ Hund exchange, undoped LaFeAsO lies just below the Fermi-liquid/non-Fermi-liquid phase boundary. Smaller U and larger J would move this point farther below this phase boundary. In the limit of one-hole doping, the system is a Mott insulator, whereas, for electron doping, Fermi-liquid properties dominate. For Ising exchange, the phase boundary is shifted to roughly 1 eV lower U values, so that U would have to be less than ~ 2 eV to preserve Fermi-liquid behavior.

Of course, in real LaFeAsO, this phase diagram should be more complicated because of the inevitable modification of the one-electron properties with doping[15,63] and because of the antiferromagnetic phase[4] observed at $n=6$. Nevertheless, the paramagnetic limit permits to draw an interesting analogy between the present multiband iron pnictide and the single-band two-dimensional Hubbard model that is frequently used to investigate Coulomb correlations in high-T_c cuprates.

Figure 11(a) shows the orbital components of the low-frequency scattering rate $\gamma_m \approx -\mathrm{Im}\,\Sigma_m(i\omega_0)$ for LaFeAsO as a function of electron doping relative to half-filling, i.e., $\delta=n/5-1$, where $n=6$ for the undoped material. As discussed above, in the limit of one-hole doping ($n=5$), the system is a Mott insulator, while for $\delta>0.2$ it becomes a weakly correlated Fermi-liquid. In the intermediate region, for $\delta<0.2$, the scattering rate increases sharply so that the system is dominated by non-Fermi-liquid properties due to the formation of frozen moments. Thus, close to $n=6$ the system is near the Fermi-liquid to non-Fermi-liquid phase boundary.

As shown in panel (b), this behavior is remarkably similar to the one found within cluster ED/DMFT for hole doping in the two-dimensional Hubbard model.[54] Analogous results have been obtained by several groups.[64–69] This model yields a Mott insulator at half-filling and exhibits a non-Fermi-liquid pseudogap phase up to a critical doping $\delta_c \approx 0.15\ldots0.2$. Ordinary metallic behavior is restored in the overdoped region, $\delta>\delta_c$. For electron doping the results are similar, except for a smaller critical doping which marks the onset of bad-metallic behavior. In view of the analogy seen in Fig. 11, the Mott phase that is relevant for LaFeAsO is not the one that should eventually appear at $n=6$ for large U, but the one that exists at realistic values of U and J at $n=5$ occupancy.

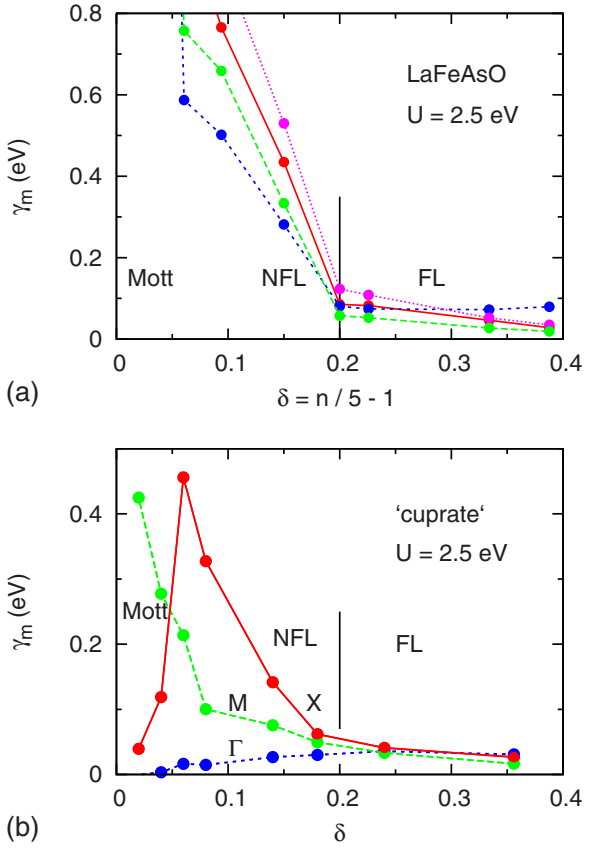

FIG. 11. (Color online) (a) Orbital-dependent scattering rates γ_m for LaFeAsO as functions of doping relative to half filling, $\delta=n/5-1$ (Hund exchange, $J=U/4$). (b) Cluster components of scattering rate for single-band two-dimensional Hubbard model as functions of hole doping (nearest and next-nearest-neighbor hopping $t=0.25$ eV and $t'=-0.075$ eV, respectively, $U=2.5$ eV and $T=0.01$ eV) (Ref. 54). The vertical bars denote the approximate doping concentrations of the Fermi-liquid to non-Fermi-liquid transition.

The results discussed above demonstrate that the Mott transition in multiorbital and multisite Hubbard models is far more complex than the paramagnetic metal to insulator transition obtained in single-band, single-site DMFT calculations. The presence of interactions channels involving orbitals or sites not only affects the overall magnitude of the critical Coulomb energy, but gives rise to a much richer phase diagram. In particular, as we have seen here for LaFeASO, a frozen-moment, non-Fermi-liquid phase emerges between the Fermi-liquid and insulating regions. Conceptually, this non-Fermi-liquid behavior is closely related to the pseudogap phase in hole-doped cuprates which arises from short-range Coulomb correlations.

IV. SUMMARY

Multiband ED/DMFT has been used to investigate the effect of correlations in the iron pnictide LaFeAsO. Starting from an accurate five-band tight-binding single-particle Hamiltonian, the many-body properties are evaluated by extending single-site ED/DMFT to five orbitals, each hybridizing with two bath levels. This scheme is particularly useful at very low temperatures, large Coulomb energies and for fully rotationally invariant Hund's rule coupling. It is shown that correlation effects in LaFeAsO give rise to a paramagnetic transition from a Fermi-liquid phase to a non-Fermi-liquid phase at a critical Coulomb energy (*pd* screened) of about 3 eV. This transition appears to be continuous and is caused by the formation of Fe 3*d* local moments. Below this transition, the quasiparticle weight of all *d* orbitals is strongly reduced and orbital polarization is less pronounced than in the uncorrelated density functional band structure. A Mott insulating phase does not appear below $U=6$ eV. For Ising exchange the Fermi-liquid to non-Fermi-liquid transition also exists, but the critical value of U is shifted to about 2 eV. Moreover, the transition appears to be first order rather than continuous.

Despite the multiband nature of LaFeAsO and the important role of exchange interactions, this system exhibits an interesting relationship to the single-band two-dimensional Hubbard model if the doping concentration is defined with respect to the half-filled 3*d* shell. Within this picture, iron pnictides and cuprates exhibit the same sequence of paramagnetic phases with increasing doping: from Mott insulator to bad metal to Fermi-liquid. Thus, fluctuations between orbitals or lattice sites lead to similar physics. According to the available experimental evidence, LaFeAsO is located on the weakly to moderately correlated side of the Fermi-liquid to non-Fermi-liquid phase boundary. Thus, iron pnictide materials appear to have two parent compounds: the antiferromagnetic semimetal at $n=6$ and the Mott insulator at $n=5$.

ACKNOWLEDGMENTS

A.L. would like to thank Igor Mazin, Luca de' Medici, and Massimo Capone for comments. The work of H.I. is supported by the Grant-in-Aid for Scientific Research (Grant No. 20540191) and by the Nihon University Strategic Projects for Academic Research. A.L.'s calculations were carried out on the Jülich Jump computer.

[1] Y. Kamihara, T. Watanabe, M. Hirano, and H. Hosono, J. Am. Chem. Soc. **130**, 3296 (2008).
[2] Z.-A. Ren, W. Lu, J. Yang, W. Yi, X.-L. Shen, Z.-C. Li, G.-C. Che, X.-L. Dong, L.-L. Sun, F. Zhou, and Z.-X. Zhao, Chin. Phys. Lett. **25**, 2215 (2008).
[3] X. H. Chen, T. Wu, G. Wu, R. H. Liu, H. Chen, and D. F. Fang, Nature **453**, 761 (2008).
[4] C. de la Cruz, Q. Huang, J. W. Lynn, J. Li, W. Ratcliff II, J. L. Zarestky, H. A. Mook, G. F. Chen, J. L. Luo, N. L. Wang, and P. Dai, Nature **453**, 899 (2008).
[5] K. Haule, J. H. Shim, and G. Kotliar, Phys. Rev. Lett. **100**, 226402 (2008).
[6] T. Yildirim, Phys. Rev. Lett. **101**, 057010 (2008).
[7] Q. Si and E. Abrahams, Phys. Rev. Lett. **101**, 076401 (2008).
[8] I. I. Mazin, D. J. Singh, M. D. Johannes, and M. H. Du, Phys. Rev. Lett. **101**, 057003 (2008).
[9] K. Kuroki, S. Onari, R. Arita, H. Usui, Y. Tanaka, H. Kontani, and H. Aoki, Phys. Rev. Lett. **101**, 087004 (2008).
[10] J. Wu, P. Phillips, and A. H. Castro Neto, Phys. Rev. Lett. **101**, 126401 (2008).
[11] M. Daghofer, A. Moreo, J. A. Riera, E. Arrigoni, D. J. Scalpino, and E. Dagotto, Phys. Rev. Lett. **101**, 237004 (2008).
[12] G. Baskaran, J. Phys. Soc. Jpn. **77**, 113713 (2008).
[13] S. Raghu, X.-L. Qi, C.-X. Liu, D. J. Scalapino, and S.-C. Zhang, Phys. Rev. B **77**, 220503(R) (2008).
[14] T. A. Maier and D. J. Scalapino, Phys. Rev. B **78**, 020514(R) (2008).
[15] I. I. Mazin, M. D. Johannes, L. Boeri, K. Koepernik, and D. J. Singh, Phys. Rev. B **78**, 085104 (2008).
[16] L. Craco, M. S. Laad, S. Leoni, and H. Rosner, Phys. Rev. B **78**, 134511 (2008).
[17] M. M. Korshunov and I. Eremin, Phys. Rev. B **78**, 140509(R) (2008).
[18] T. Miyake, L. Pourovskii, V. Vildosola, S. Bierman, and A. Georges, J. Phys. Soc. Jpn. **77**, Suppl. C, 99 (2008).
[19] K. Nakamura, R. Arita, and M. Imada, J. Phys. Soc. Jpn. **77**, 093711 (2008).
[20] A. O. Shorikov, M. A. Korotin, S. V. Streltsov, D. M. Korotin, V. I. Anisimov, and S. L. Skornyakov, arXiv:0804.3283 (unpublished).
[21] V. I. Anisimov, D. M. Korotin, M. A. Korotin, A. V. Kozhevnikov, J. Kunes, A. O. Shorikov, S. L. Skornyakov, and S. V. Streltsov, J. Phys.: Condens. Matter **21**, 075602 (2009).
[22] V. Vildosola, L. Pourovskii, R. Arita, S. Biermann, and A. Georges, Phys. Rev. B **78**, 064518 (2008).
[23] M. S. Laad, L. Craco, S. Leoni, and H. Rosner, Phys. Rev. B **79**, 024515 (2009).
[24] S. Graser, T. A. Maier, P. J. Hirschfeld, and D. J. Scalpino, New J. Phys. **11**, 025016 (2009).
[25] K. Haule and G. Kotliar, New J. Phys. **11**, 025021 (2009).
[26] A. Hackl and M. Wojta, New J. Phys. **11**, 055064 (2009).
[27] L. de'Medici, S. R. Hassan, and M. Capone, J. Supercond. Novel Magn. **22**, 535 (2009).
[28] S.-P. Kou, T. Li, and Z.-Y. Weng, Europhys. Lett. **88**, 17010 (2009).
[29] R. Yu, K. T. Trinh, A. Moreo, M. Daghofer, J. A. Riera, S. Haas, and E. Dagotto, Phys. Rev. B **79**, 104510 (2009).
[30] K. Kuroki, H. Usui, S. Onari, R. Arita, and H. Aoki, Phys. Rev. B **79**, 224511 (2009).
[31] W. L. Yang, A. P. Sorini, C.-C. Chen, B. Moritz, W.-S. Lee, F. Vernay, P. Olalde-Velasco, J. D. Denlinger, B. Delley, J.-H. Chu, J. G. Analytis, I. R. Fisher, Z. A. Ren, J. Yang, W. Lu, Z. X. Zhao, J. van den Brink, Z. Hussain, Z.-X. Shen, and T. P. Devereaux, Phys. Rev. B **80**, 014508 (2009); See also, Z. Tesanovic, Physics **2**, 60 (2009).
[32] M. Aichhorn, L. Pourovskii, V. Vildosola, M. Ferrero, O. Parcol-

let, T. Miyake, A. Georges, and S. Biermann, Phys. Rev. B **80**, 085101 (2009).
[33] S. L. Skornyakov, A. V. Efremov, N. A. Skorikov, M. A. Korotin, Yu. A. Izyumov, V. I. Anisimov, A. V. Kozhevnikov, and D. Vollhardt, Phys. Rev. B **80**, 092501 (2009).
[34] M. M. Qazilbash, J. J. Hamlin, R. E. Baumbach, L. Zhang, D. J. Singh, M. B. Maple, and D. N. Basov, Nat. Phys. **5**, 647 (2009).
[35] L. Hozoi and P. Fulde, Phys. Rev. Lett. **102**, 136405 (2009).
[36] Q. Si, E. Abrahams, J. Dai, and J.-X. Zhu, New J. Phys. **11**, 045001 (2009); Q. Si, Nat. Phys. **5**, 629 (2009).
[37] R. Arita and H. Ikeda, J. Phys. Soc. Jpn. **78**, 113707 (2009).
[38] M. Daghofer, A. Nicholson, A. Moreo, and E. Dagotto, Phys. Rev. B **81**, 014511 (2010).
[39] S. Zhou and Z. Wang, arXiv:0910.2707 (unpublished).
[40] I. I. Mazin, arXiv:0910.4117 (unpublished).
[41] A. Georges, G. Kotliar, W. Krauth, and M. J. Rozenberg, Rev. Mod. Phys. **68**, 13 (1996).
[42] M. Caffarel and W. Krauth, Phys. Rev. Lett. **72**, 1545 (1994).
[43] E. Dagotto, Rev. Mod. Phys. **66**, 763 (1994).
[44] P. Werner, E. Gull, M. Troyer, and A. J. Millis, Phys. Rev. Lett. **101**, 166405 (2008).
[45] T. Pruschke and R. Bulla, Eur. Phys. J. B **44**, 217 (2005).
[46] A. Liebsch, Phys. Rev. Lett. **95**, 116402 (2005).
[47] C. Cao, P. J. Hirschfeld, and H.-P. Cheng, Phys. Rev. B **77**, 220506(R) (2008).
[48] D. J. Singh and M.-H. Du, Phys. Rev. Lett. **100**, 237003 (2008).
[49] A. Liebsch and H. Ishida, Eur. Phys. J. B **61**, 405 (2008).
[50] A. Liebsch and H. Ishida, Phys. Rev. Lett. **98**, 216403 (2007).
[51] C. A. Perroni, H. Ishida, and A. Liebsch, Phys. Rev. B **75**, 045125 (2007).
[52] A. Liebsch, Phys. Rev. B **77**, 115115 (2008); H. Ishida and A. Liebsch, *ibid.* **77**, 115350 (2008).
[53] A. Liebsch, H. Ishida, and J. Merino, Phys. Rev. B **78**, 165123 (2008).
[54] A. Liebsch and N.-H. Tong, Phys. Rev. B **80**, 165126 (2009).
[55] R. B. Lehoucq, D. C. Sorensen, and C. Yang, *ARPACK Users' Guide* (SIAM, Philadelphia, 1997).
[56] D. H. Lu, M. Yi, S.-K. Mo, A. S. Erickson, J. Analytis, J.-H. Chu, D. J. Singh, Z. Hussain, T. H. Geballe, I. R. Fisher, and Z.-X. Shen, Nature (London) **455**, 81 (2008).
[57] H. Ding, P. Richard, K. Nakayama, K. Sugawara, T. Arakane, Y. Sekiba, A. Takayama, S. Souma, T. Sato, T. Takahashi, Z. Wang, X. Dai, Z. Fang, G. F. Chen, J. L. Luo, and N. L. Wang, Eur. Phys. Lett. **83**, 47001 (2008).
[58] In Ref. 5, a Mott insulator was found at $U=4.5$ eV, $J=0.7$ eV, while in Ref. 20 even $U=5$ eV did not yield a Mott phase.
[59] A. M. Läuchli and P. Werner, Phys. Rev. B **80**, 235117 (2009).
[60] A. Liebsch, Phys. Rev. B **70**, 165103 (2004).
[61] T. A. Costi and A. Liebsch, Phys. Rev. Lett. **99**, 236404 (2007).
[62] S. Biermann, L. de'Medici, and A. Georges, Phys. Rev. Lett. **95**, 206401 (2005).
[63] G. Xu, H. Zhang, X. Dai, and Z. Fang, EPL **84**, 67015 (2008).
[64] M. Jarrell, Th. Maier, M. H. Hettler, and A. N. Tahvildarzadeh, Europhys. Lett. **56**, 563 (2001).
[65] D. Sénéchal and A.-M. S. Tremblay, Phys. Rev. Lett. **92**, 126401 (2004).
[66] O. Parcollet, G. Biroli, and G. Kotliar, Phys. Rev. Lett. **92**, 226402 (2004).
[67] H. Park, K. Haule, and G. Kotliar, Phys. Rev. Lett. **101**, 186403 (2008).
[68] N. S. Vidhyadhiraja, A. Macridin, C. Sen, M. Jarrell, and M. Ma, Phys. Rev. Lett. **102**, 206407 (2009).
[69] Ph. Werner, E. Gull, O. Parcollet, and A. J. Millis, Phys. Rev. B **80**, 045120 (2009).